Estimating the Fraction of PAR Absorbed by Live Phytoplankton from Satellite Data

Robert Frouin, Jing Tan, B. Greg Mitchell

Scripps Institution of Oceanography
University of California San Diego
La Jolla, California, USA

MODIS/VIIRS Meeting, College Park, Maryland, 19 November 2019

Introduction

-*APAR*, is the fraction of incoming solar radiation in the *PAR* spectral region (400-700 nm) that is absorbed by active (live) photosynthetic organisms present in the euphotic layer.

-This biophysical variable controls the growth of phytoplankton and regulates the composition and evolution of marine ecosystems.

-Knowing the distribution of *APAR* over the oceans, spatially and temporally, is critical to understanding biogeochemical cycles of carbon, nutrients, and oxygen, documenting the response of marine ecosystems to climate change, and investigating the fate of anthropogenic atmospheric carbon dioxide.

Introduction (cont.1)

-Primary production, *PP*, depends on the fraction of photosynthetically available radiation, *PAR*, absorbed by live phytoplankton, *APAR*, i.e., $PP = e\ APAR\ PAR$, where *e* is an efficiency factor for photosynthesis.

-*APAR* can be expressed as (Kirk 1994):

$$APAR=\int\int\{K_d(\lambda,z)E_d(\lambda,z)\ a_{ph}(\lambda,z)/a_{tot}(\lambda,z)\}d\lambda dz / \int E_d(\lambda,0^-)\ d\lambda$$

where K_d is the diffuse attenuation coefficient, E_d is the spectral solar irradiance below the surface, a_{ph} is the phytoplankton absorption coefficient, a_{tot} is the total absorption coefficient, and the integral is over the PAR spectral range, i.e., 400 to 700 nm, and over the depth z (from surface to the depth of the euphotic zone).

-In the case of a vertically homogeneous water body, *APAR* reduces to:

$$APAR=\int(E_d(\lambda)\ a_{ph}(\lambda)/a_{tot}(\lambda))d\lambda / \int E_d(\lambda)d\lambda$$

Introduction (cont.2)

-Computing *APAR* requires knowledge of $E_d(\lambda)$, $K_d(\lambda)$, $a_{ph}(\lambda)$, and $a_{tot}(\lambda)$.

-$E_d(\lambda)$ can be obtained by adapting existing methods for *PAR* above the surface. This is straightforward since the effect of clouds on transmittance is fairly white in the PAR spectral range (see Frouin et al., Front. Mar. Sci., 2018).

-$K_d(\lambda)$, $a_p(\lambda)$, and $a_{tot}(\lambda)$ can be obtained from water reflectance, $R_w(\lambda)$, using various techniques; see, e.g., IOCCG, 2005 for absorption coefficients.

-Estimating the various quantities from R_w is accomplished with uncertainties (it is especially difficult to estimate a_{ph}); no vertical information. Algorithms are also sensitive to atmospheric correction errors.

Algorithm Development

-Consider homogeneous case for simplicity. *APAR* can be re-arranged in terms of R_w as:

$$APAR \approx \int\{E_d(0^-)\,[a_{ph}/(a_{ph} + a_{dm} + a_g)]\,[1 - (R_w(0^-)/R_{w0}(0^-))(f_0/f)(b_{b0}/(b_{b0} + b_{bp})]\}d\lambda \,/\, \int E_d(0^-)\,d\lambda$$

by incorporating the following equations:

$$a_{tot} = a_{ph} + a_{dm} + a_g + a_0,\; R_{w0}(0^-) \approx f_0 b_{b0}/a_0,\; R_w(0^-) \approx f b_b/a_{tot}$$

where a_{dm}, a_g and a_0 are the absorption coefficients for detritus/sediments, colored dissolved organic matter, and pure water, respectively, b_{b0} and b_{bp} are the backscattering coefficients for water molecules and particles, respectively, and R_{w0} is the reflectance for pure sea water.

-This suggests that *APAR* can be approximated by a linear combination of $R_w(0^-)/R_{w0}(0^-)$in the PAR spectral range. Introducing R_{w0} reduces the sensitivity to IOP variability.

Dependence of APAR on [Chl] and $R_w(0-)/R_{w0}(0-)$, Case 1 waters

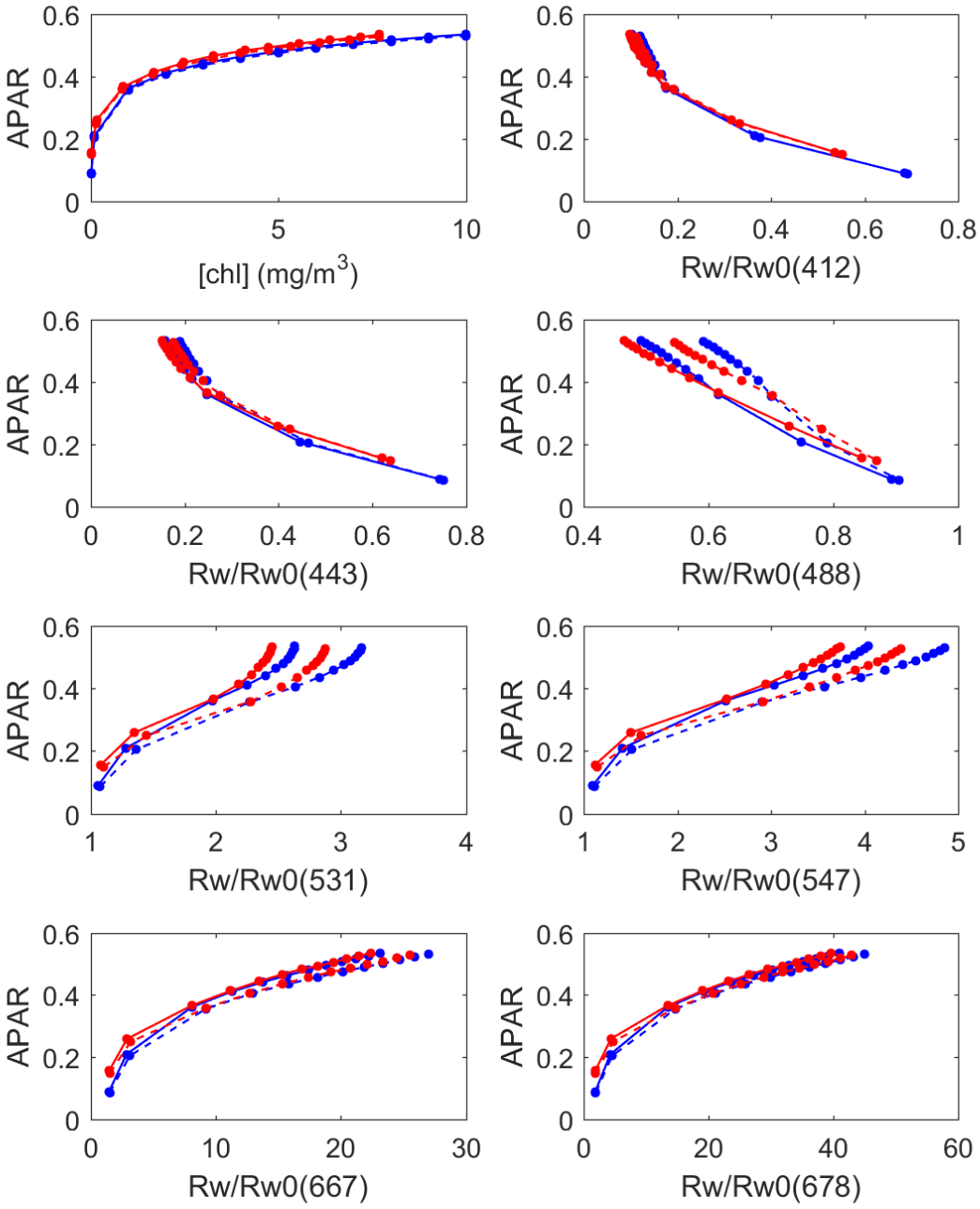

Figure 1: *Dependence of APAR on [Chl] and $R_w(0-)/R_{w0}(0-)$ for typical Case 1 waters, either vertically homogeneous (blue) or heterogeneous (red). Solar zenith angle is 30° (solid line) and 60° (dashed line).*

Estimated vs. theoretical APAR, various algorithms

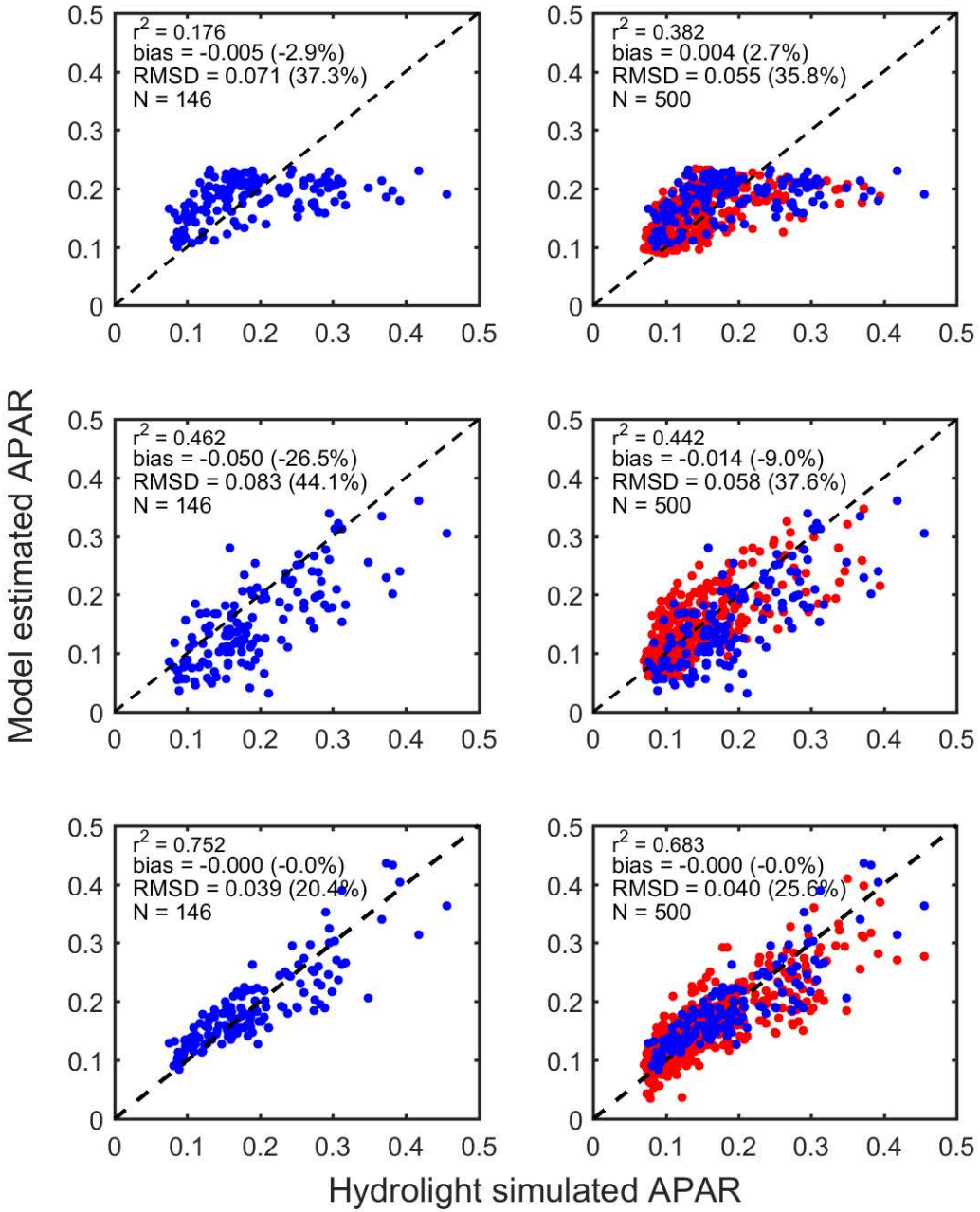

***Figure 2**: Comparison of estimated and theoretical (Hydrolight-simulated) APAR for Case 1 waters (left) and Case 1 + Case 2 waters (right). Data set is from IOCCG (2006). Top row: using OCM3-derived [chl] and APAR = a[chl]^b; Middle row: using QAA-derived a_{ph} and a_{tot}; Bottom row: using R_w/R_{w0} ratios at 412, 443, 488, 531, and 547 nm.*

Field data

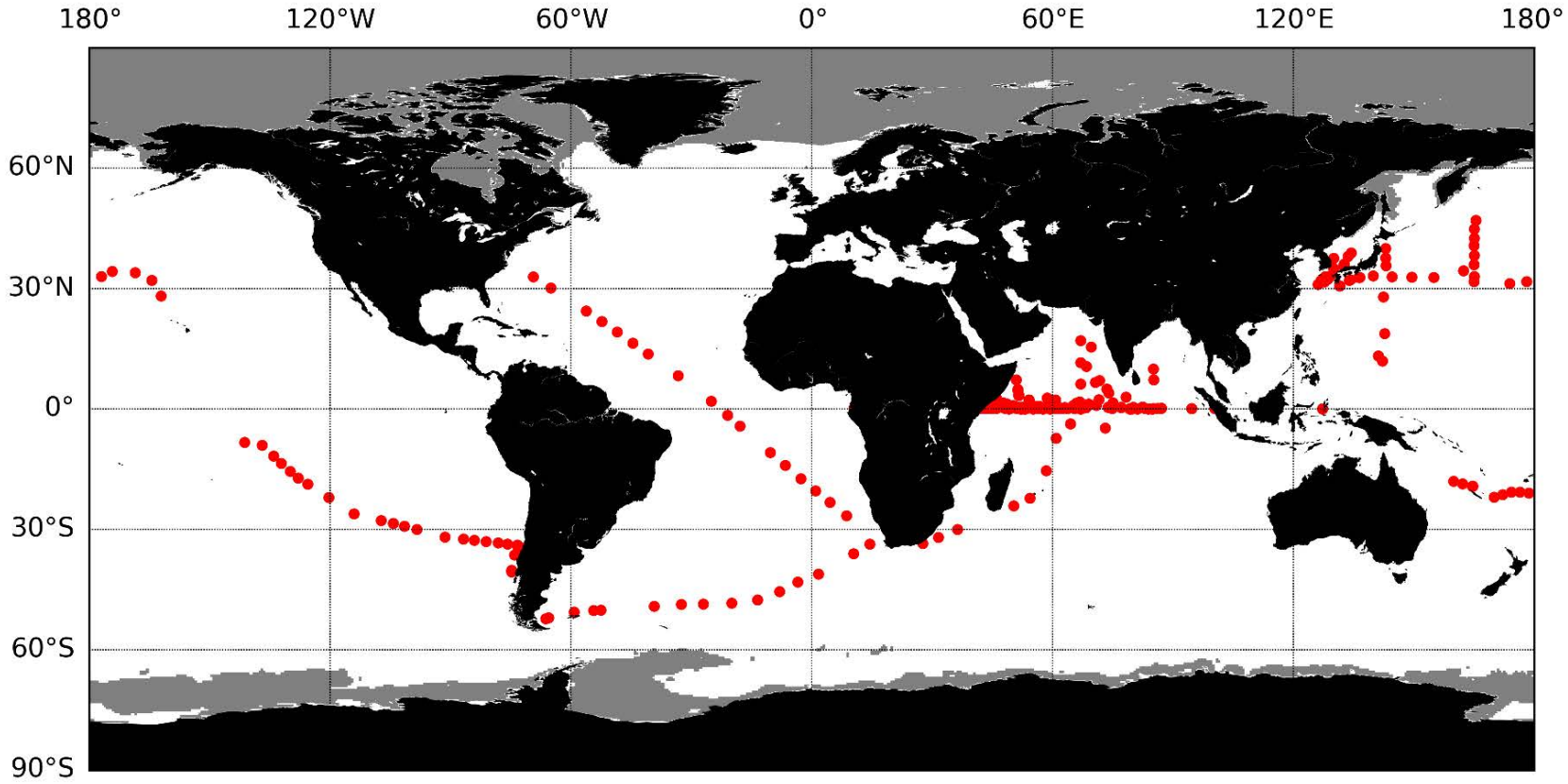

***Figure 3**: Geographic location of 336 in situ sampling stations with E_d, $a_{ph,}$ and a_{tot} profiles and R_w measurements. Data are from the SIO SPG archive and BIOSOPE, OUTPACE, Japan Sea, Aerosols99, and Southern Ocean cruises.*

APAR versus R_w/R_{w0} from field data

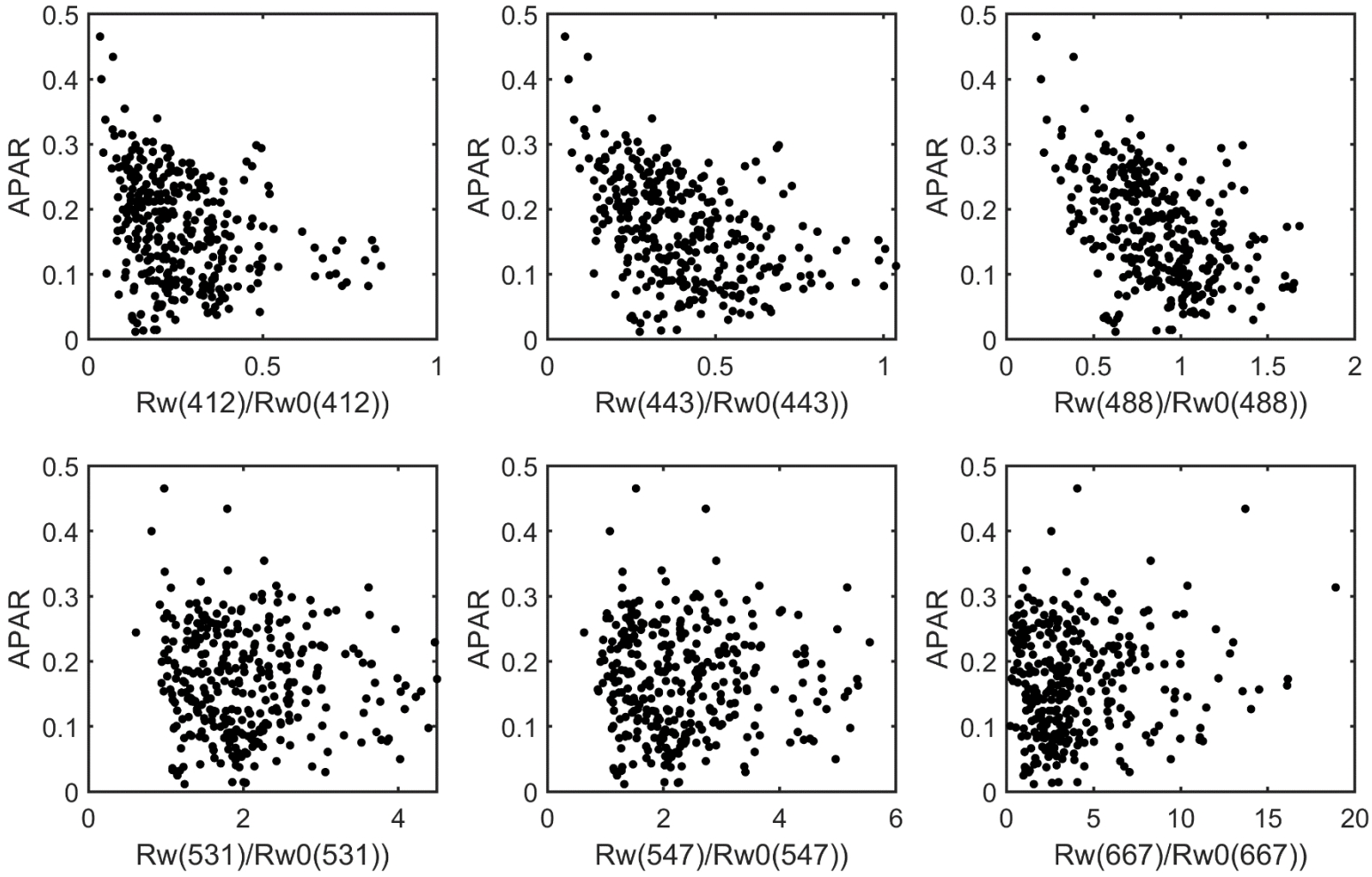

***Figure 4**: Relation between APAR versus(R_w/R_{w0} at MODIS wavelengths from field data (SPG archive, other cruises, 336 points).*

Performance of linear R_w/R_{w0} combinations

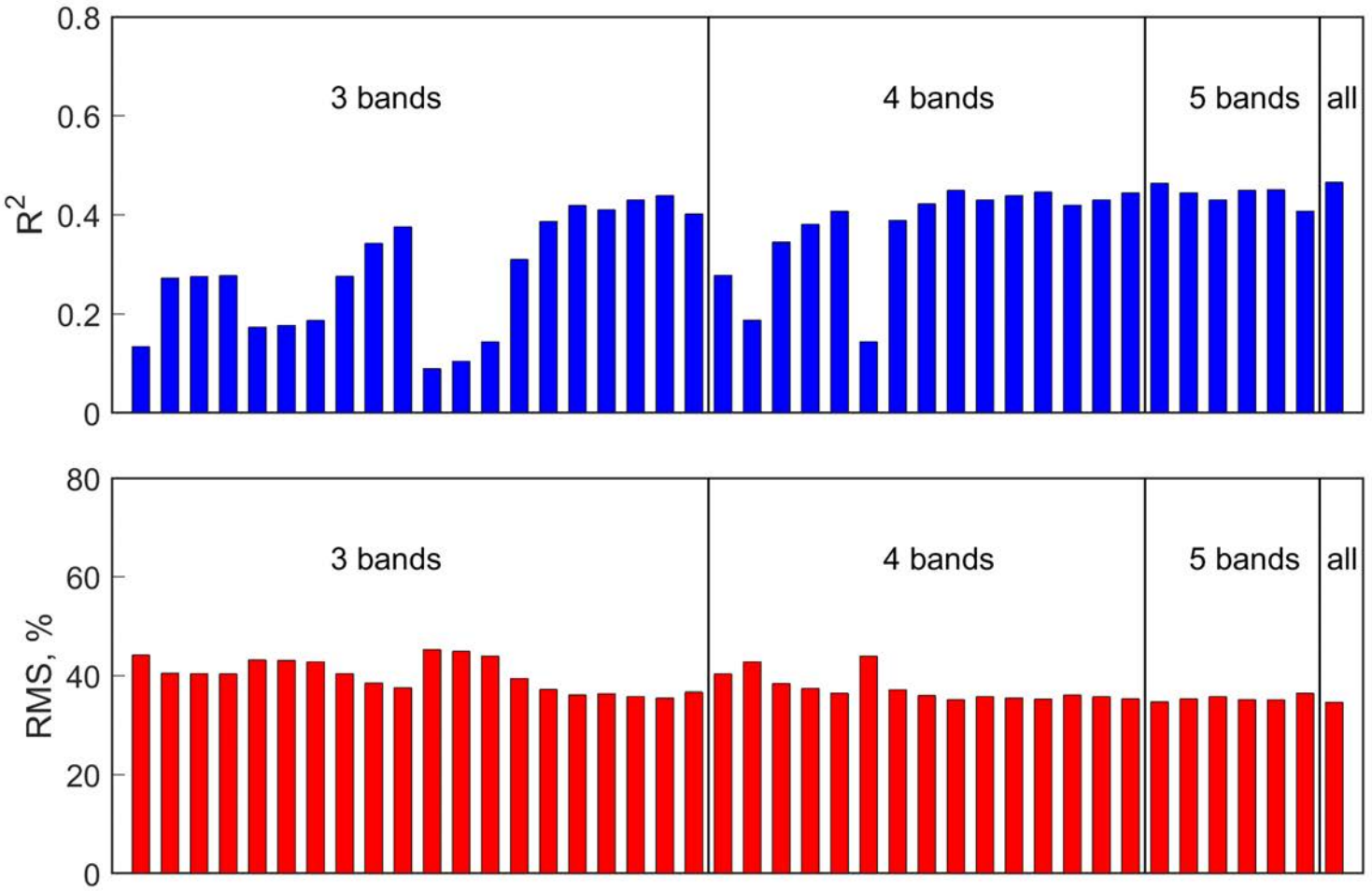

***Figure 5**: R^2 and RMS (%) of estimated APAR using 3-band, 4-band, 5-band, and 6-band combinations when applying systematical examination to in-situ data. APAR is estimated as linear combinations of R_w/R_{w0}. MODIS bands at 412, 443, 488, 531, 547, and 667 are considered.*

Comparison of APAR algorithms ([Chl]-based, QAA-based, and linear R_w /R_{w0} combination)

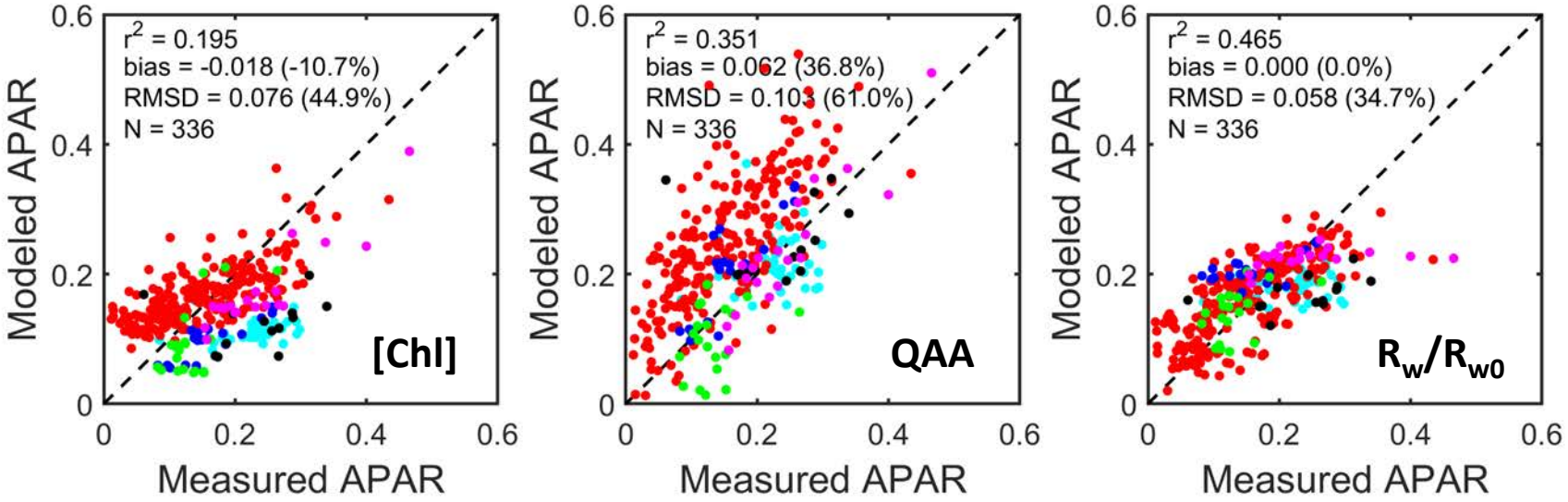

***Figure 6**: Comparison of estimated and "measured" APAR using field data archived in the SPG database (red), collected during BIOSOPE (blue), OUTPACE (green), Japan Sea (black), Aerosols99 (cyan) and Southern Ocean (magenta) cruises: left - using OC3M-derived [chl] and APAR = a[Chl]^b, middle - using QAA-derived a_{ph} and a_{tot}, and right - using R_w /R_{w0} ratios at 412, 443, 488, 531, 547, and 667 nm.*

-Accuracy is substantially improved using R_w /R_{w0} combination, e.g., RMSD reduced from 61 to 34% compared with QAA-based method.

-To improve *APAR* estimates, one may classify reflectance spectra, and for each class use a separate linear R_w/R_{w0} combination.

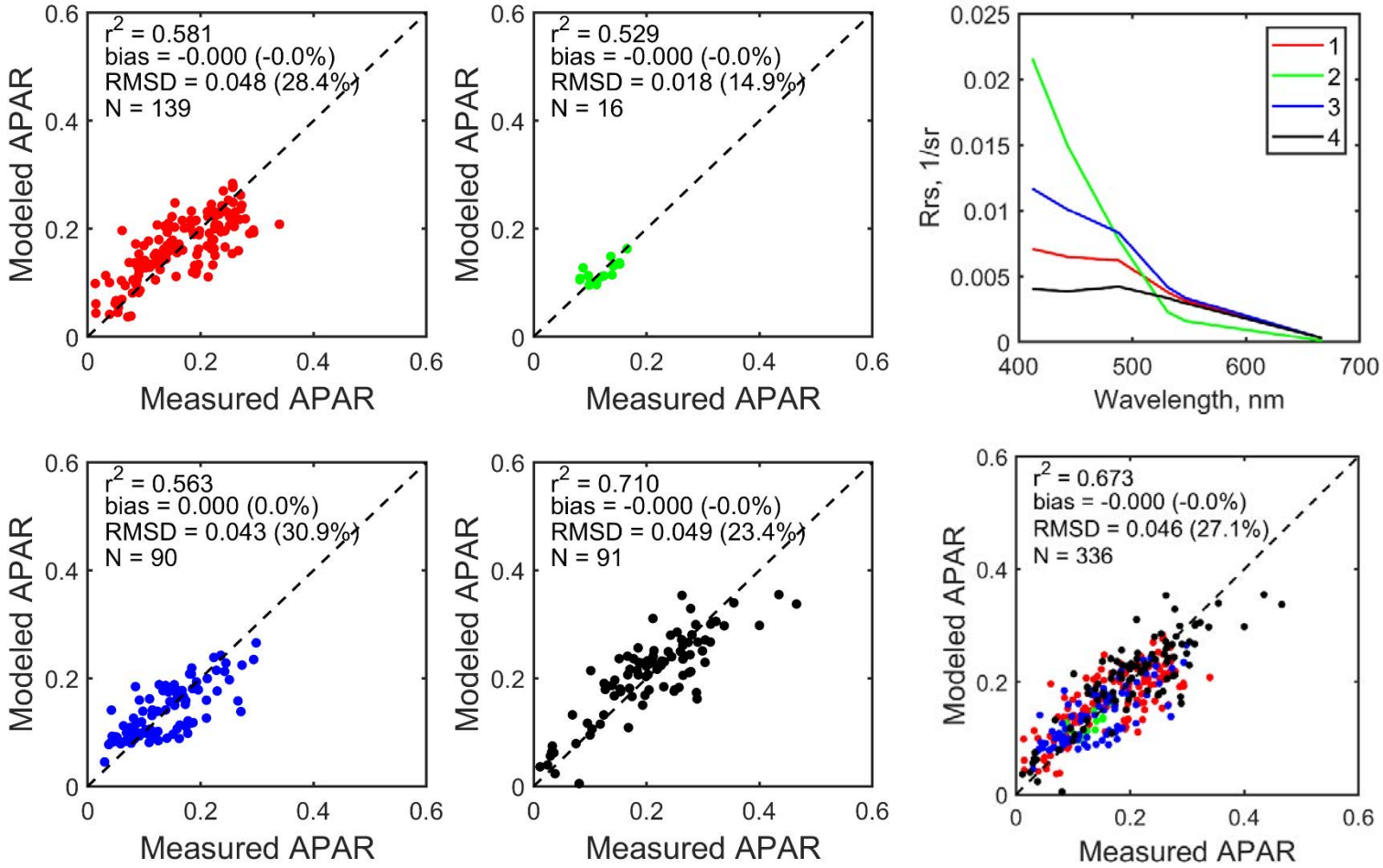

***Figure 7**: Top right: Average reflectance spectra for 4 classes obtained using k-means. Left: Modeled versus measured APAR for each class. The coefficients of estimating APAR are determined based on specific water class, using all 6 bands. Right: Modeled versus measured APAR, all four water classes together. RMSD is reduced from 35 to 27% and R^2 is increased from 0.46 to 0.67 when using classification.*

Robustness of R_w/R_{wO} algorithm to atmospheric correction errors

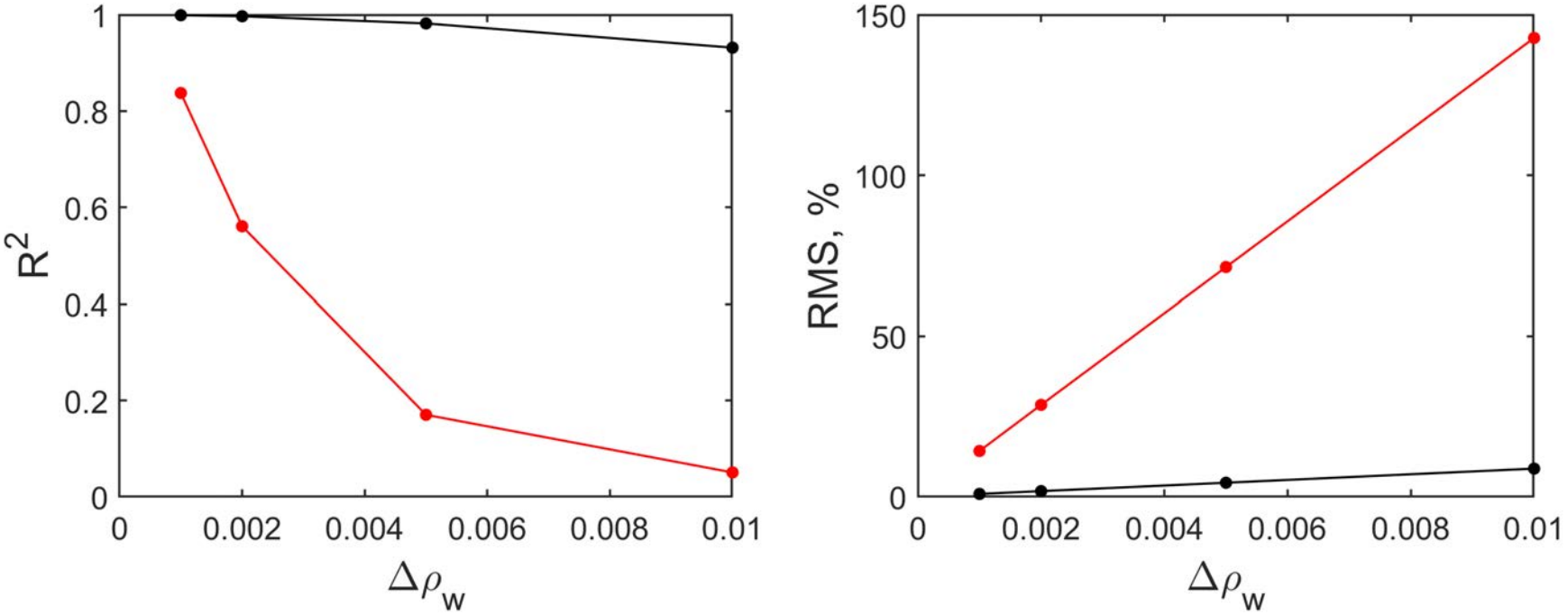

***Figure 8**: Sensitivity of the best linear combination (i.e., using 6 bands) to atmospheric noise, which is spectrally correlated (black) and uncorrelated (red). The noise level at 443 nm, $\Delta\rho_w$ (ρ_w is the water reflectance above surface), varies from 0.001 to 0.01.*

R_w/R_{w0} algorithm and uncertainty for satellite application

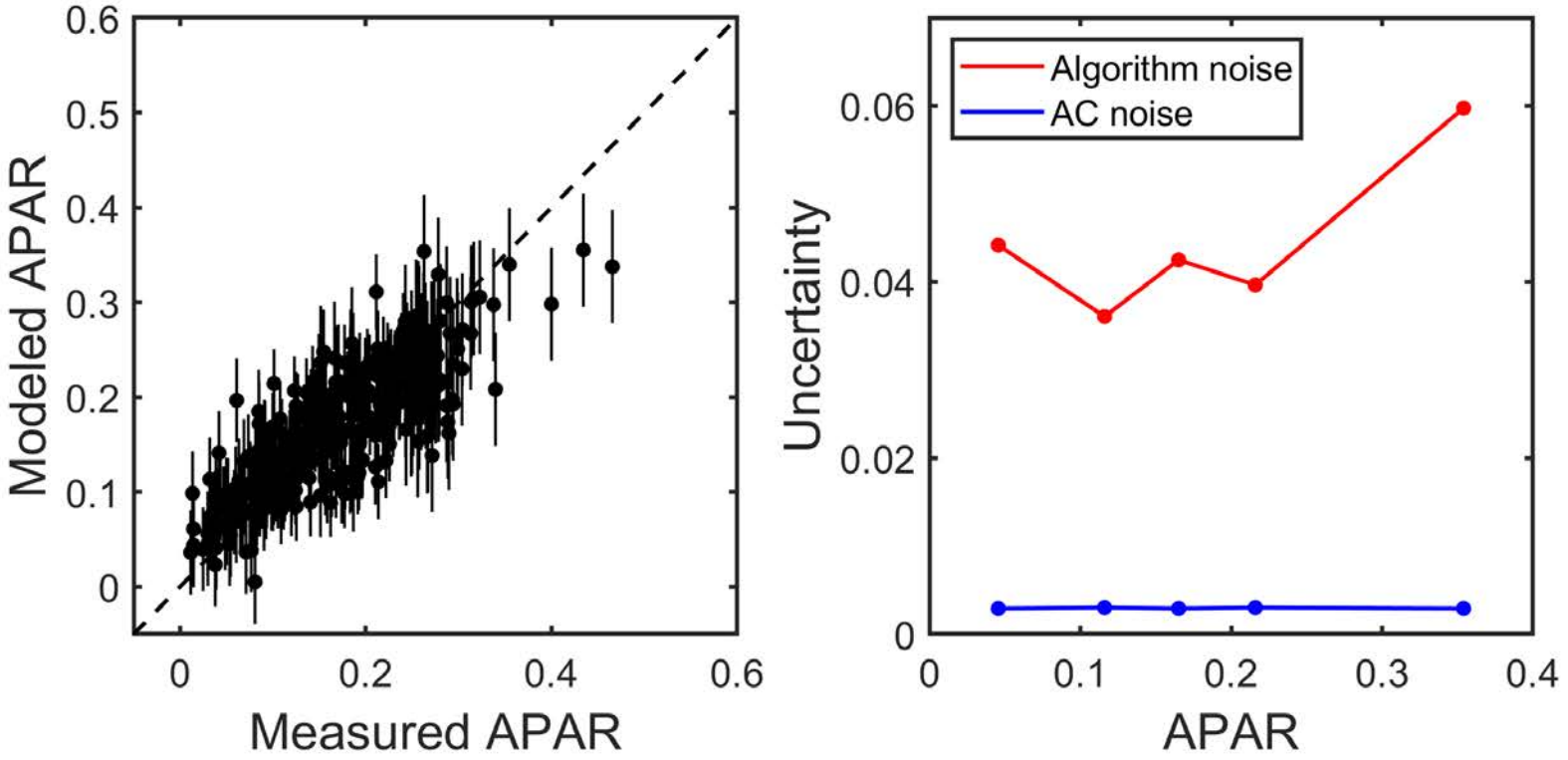

***Figure 9**: Left: comparison of estimated and "measured" APAR using field measurements. Error bars indicate the noise due to spectrally correlated atmospheric noise (±0.001 on ρ_w at 443 nm) and algorithm error. Right: APAR uncertainty due to spectrally correlated atmospheric correction noise (blue) and algorithm error (red). APAR=0.1084+1.8385$R_w(412)/R_{w0}(412)$-2.1448$R_w(443)/R_{w0}(443)$+0.5785*$R_w(488)/R_{w0}(488)$-0.1935$R_w(531)/R_{w0}(531)$+0.1141$R_w(547)/R_{w0}(547)$-0.0008$R_w(667)/R_w(667)$.*

Application to L2 MODIS imagery, Patagonia, March 26, 2019

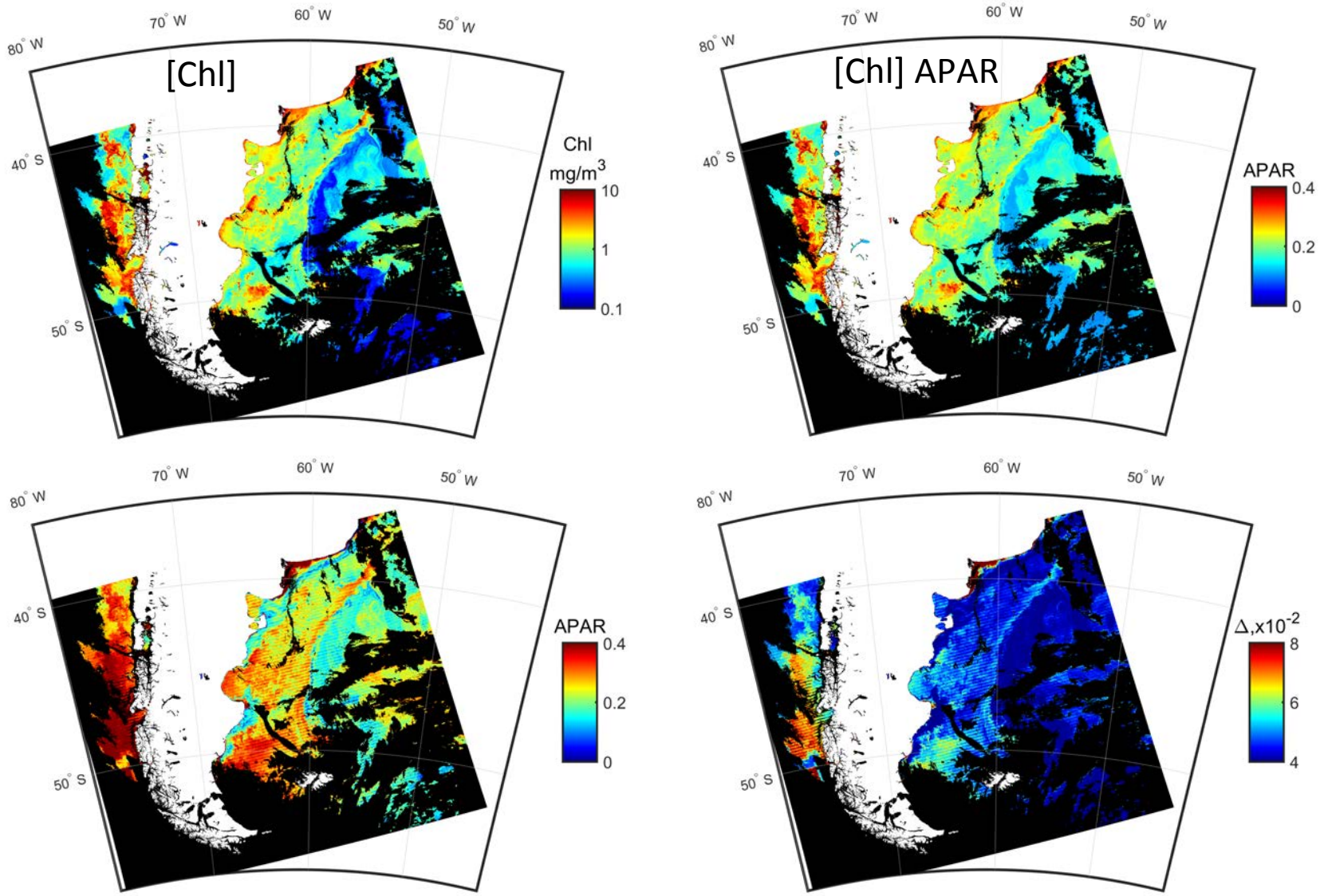

***Figure 10**: Application of APAR algorithms to MODIS-A imagery of March 26, 2019. Top left: [Chl]; Top right: [Chl]-based APAR; Bottom left: R_w/R_{wO}-based APAR; Bottom right: uncertainty on R_w/R_{wO}-based APAR. Land is in white and missing data in black.*

Average APAR from MODIS global L3 imagery, March 2018

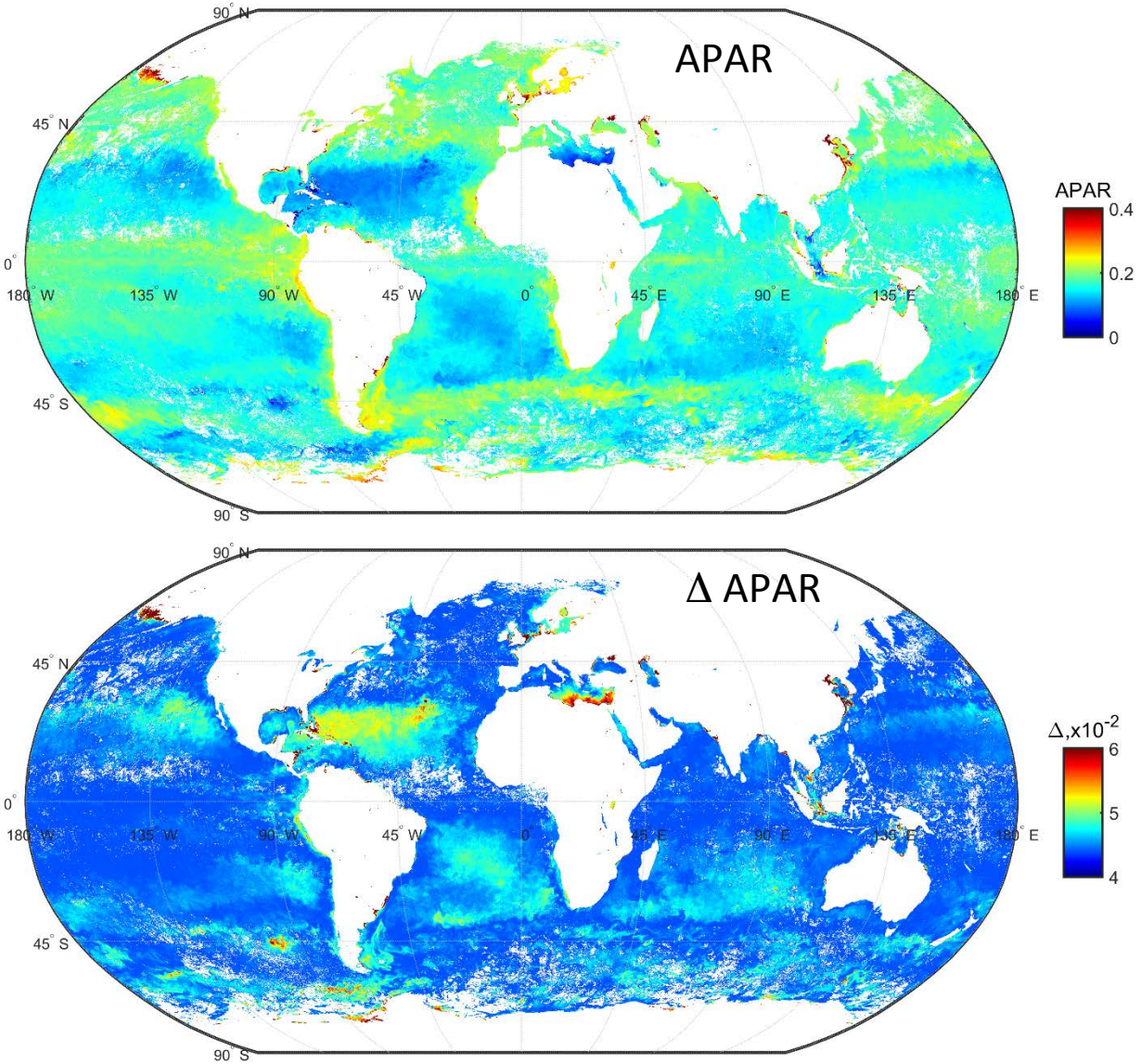

***Figure 11**: Monthly average APAR (March 2018) estimated from MODIS L3 imagery by the R_w/R_{w0} algorithm and associated uncertainty (top and bottom, respectively).*

Relative frequency, [Chl] and linear R_w/R_{w0} combination algorithms

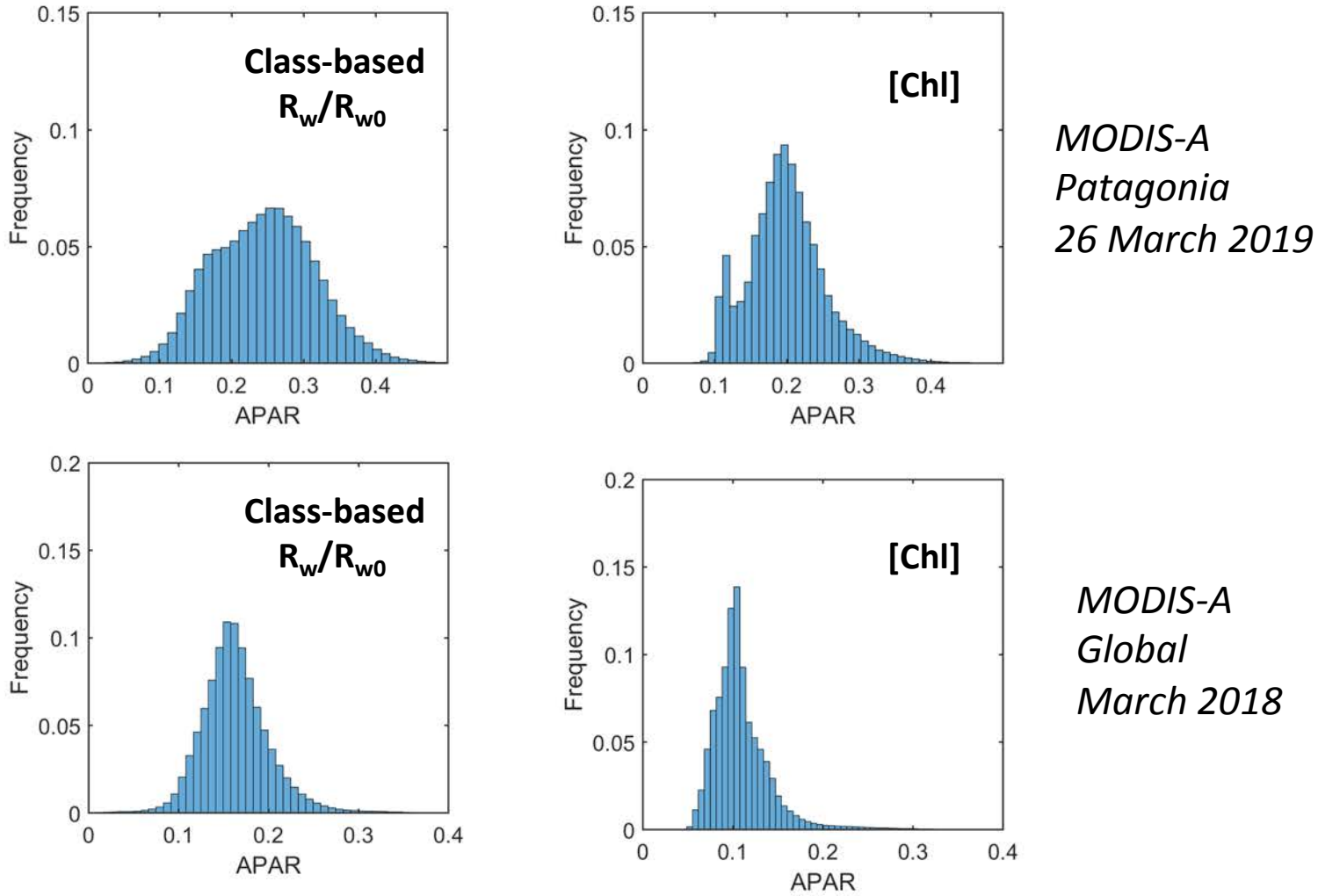

***Figure 12**: Relative frequency histograms for [Chl] and class-based R_w/R_{w0} algorithms applied to MODIS data. Top: Patagonia, 26 March 2019; Bottom: Global, March 2018.*

Application of APAR algorithm to EPIC imagery, 01/01/2018

EPIC APAR

EPIC APAR uncertainty

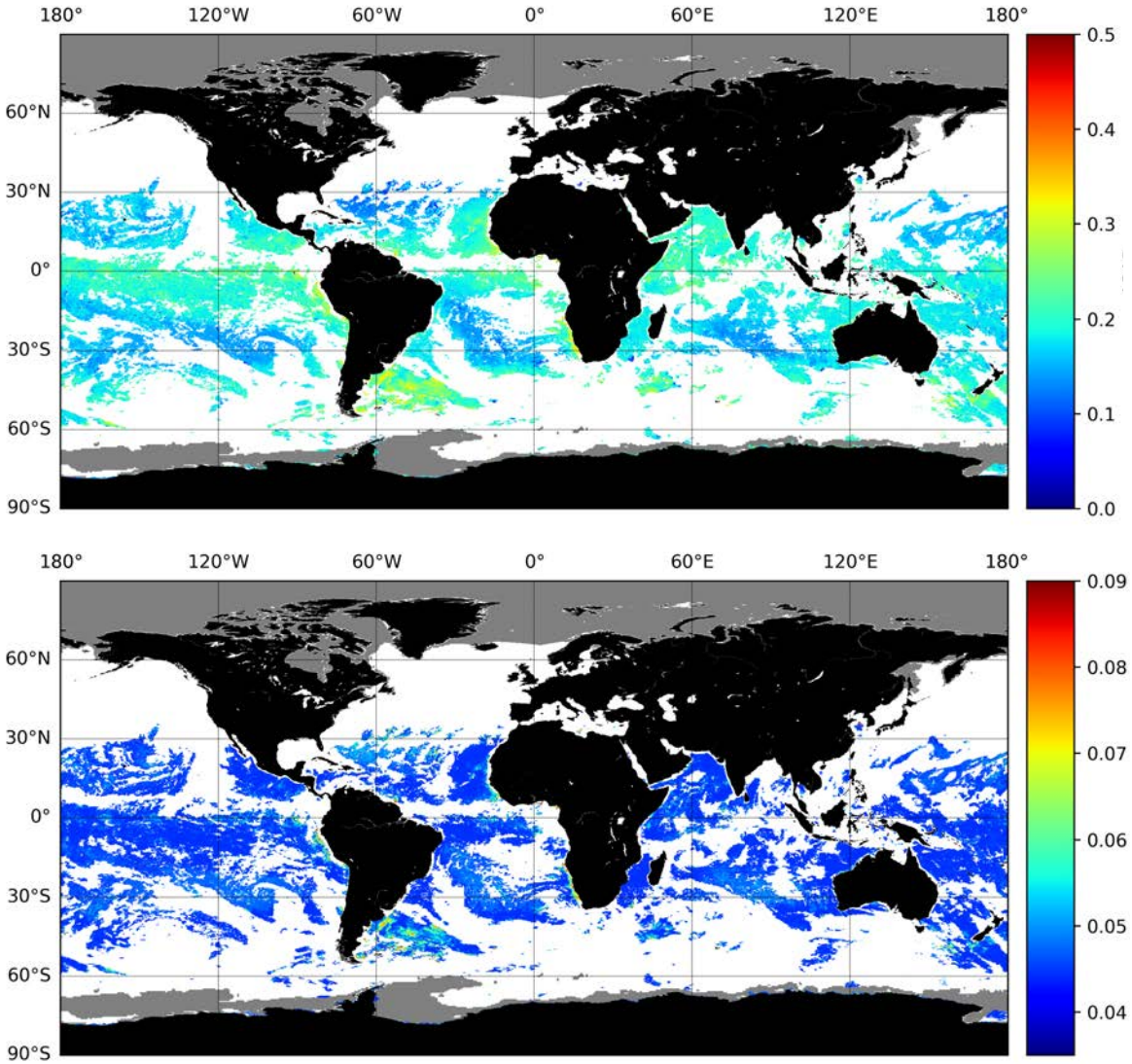

***Figure 13**: Estimated APAR from EPIC imagery acquired on January 1, 2018 using linear combination of R_w/R_{w0} at 443, 551, and 680 nm after R_w classification (top) and associated uncertainty (bottom).*

Class-based R_w/R_{w0} algorithm performance

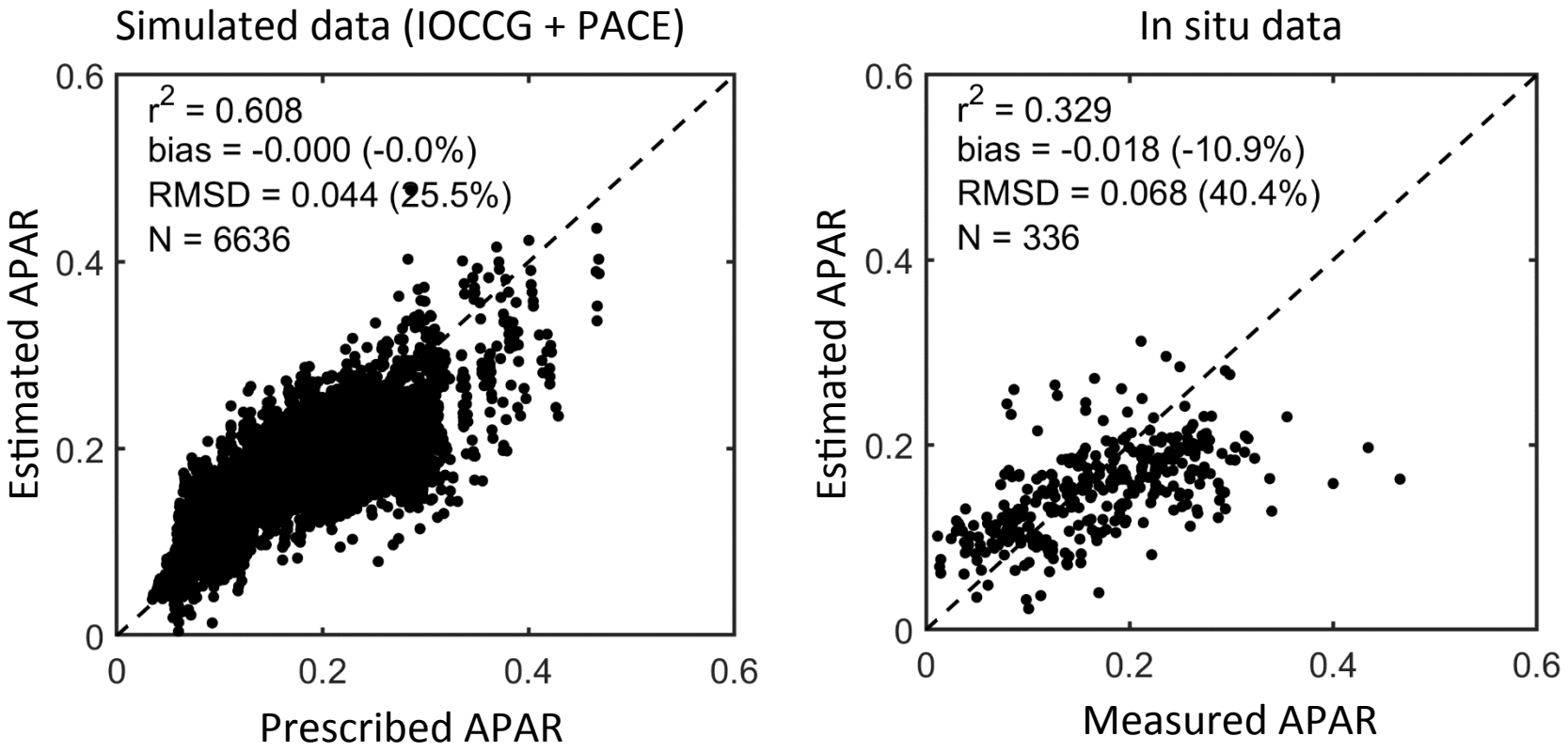

***Figure 14**: Theoretical performance of class-based APAR linear R_w/R_{w0} algorithm on simulated data (6636 cases), 8 classes (left) and evaluation on in situ data (336 points) (right). IOCCG + PACE data set is used for IOPs with various Sun zenith angles and vertical profiles (homogeneous and heterogeneous).*

Machine learning algorithm performance

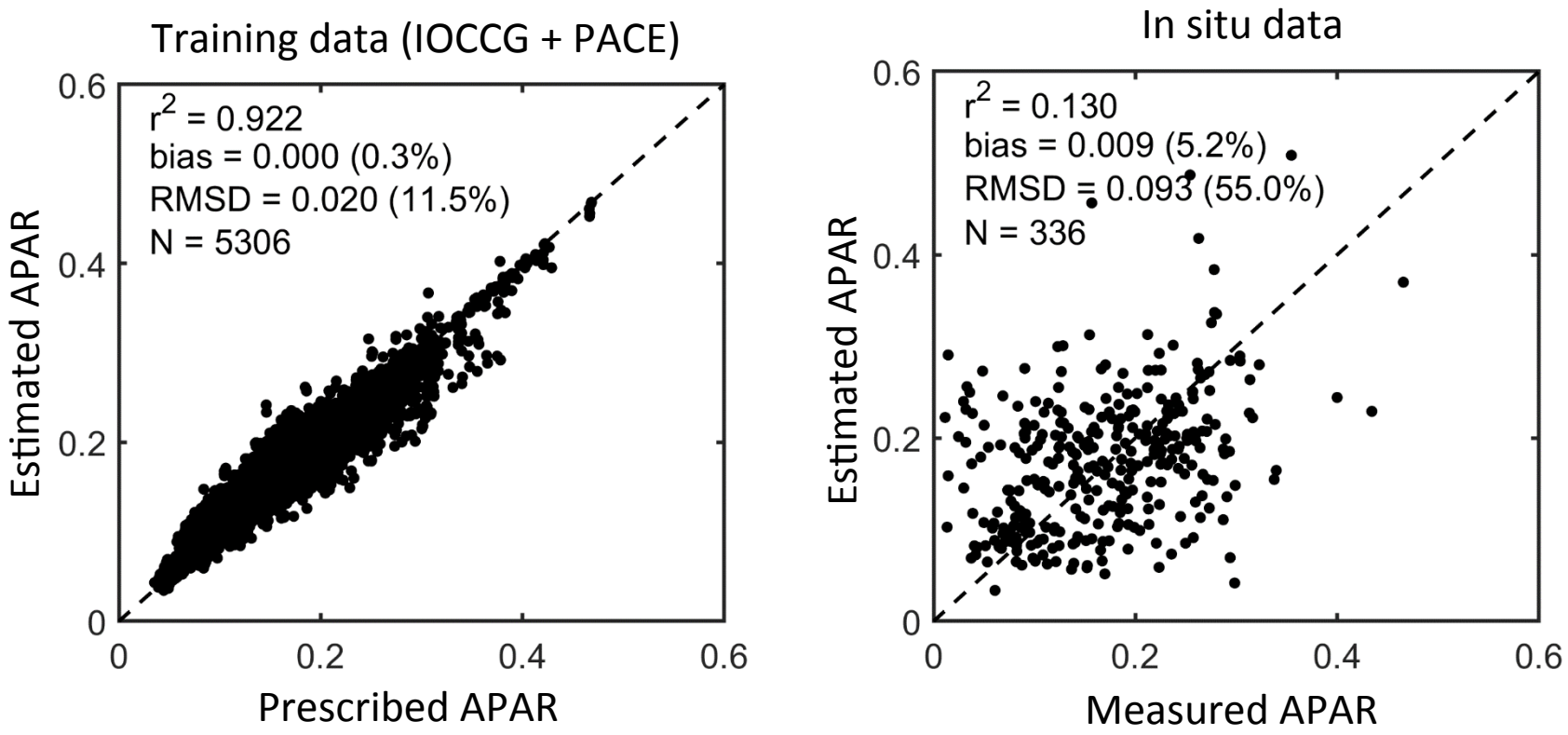

***Figure 15**: Same as Figure 14, but class-based neural network algorithm. Theoretical performance is improved, but performance on in situ data is degraded.*

PCA-based algorithm performance

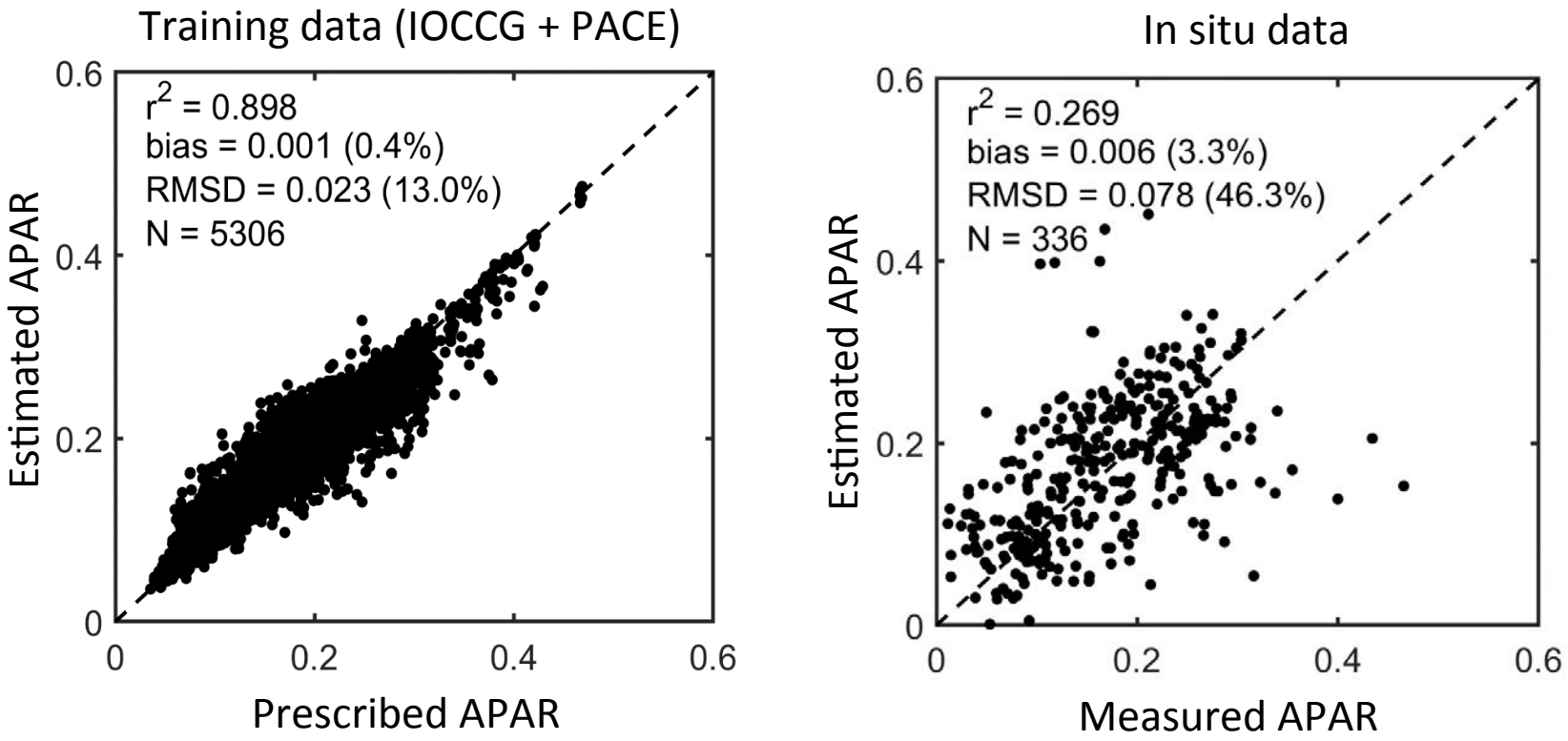

***Figure 16**: Same as Figure 14, but class-based PCA-based algorithm. Only PCs most correlated to APAR are used to map APAR via neural network. Performance on in situ data is better than with machine learning algorithm.*

Summary/Conclusions

-APAR can be derived directly from a linear combination of R_w/R_{w0} in the PAR spectral range. Spectral absorption coefficients, K_d, and E_d do not need to be determined, therefore errors in the determination of these coefficients is avoided.

-For MODIS, and based n in situ data, 6 spectral bands (412, 443, 488, 531, 547, and 667) yields the most accurate estimates.

-Accuracy is improved compared with *[Chl]*- and QAA-based algorithms, e.g., RMS difference reduced to 34% instead of 42 and 67%, respectively.

-Algorithm is robust to spectrally correlated atmospheric correction errors.

-Classifying reflectance and using a linear R_w/R_{w0} combination for each class is promising to reduce the impact of IOP variability and improve APAR estimates. RMS difference is reduced to 27%.

Summary/Conclusions (cont.)

-A more comprehensive in situ dataset is needed to generalize the results. Simulations may fill data gaps, and allow more robust APAR determinations per class.

-Other algorithms may be envisioned to improve estimates, e.g., principal component (PC) analysis to select PCs best correlated to APAR, or machine learning, the subject of future work.